 FDMP, vol.6, no.3, pp.251-275, 2010

Magnetohydrodynamics Stability of Natural Convection During Phase Change of Molten Gallium in a Three-Dimensional Enclosure

S. Bouabdallah[1,2] **and R. Bessaïh**[1]

Abstract: In this paper, a numerical study of magnetohydrodynamics stability during phase change of a pure metal (liquid Gallium) in a cubical enclosure is presented. An external magnetic field is applied in X-, Y-, and Z-directions separately. Two electric potential boundary conditions are considered: electrically conducting and insulating walls. The finite-volume method with enthalpy formulation is used to solve the mathematical model in the solid and liquid phases. The Grashof number is fixed at Gr =10^5 and the Hartmann number is varied from Ha= 0 to 200. The effect of magnetic field on the flow field and heat transfer, and on the interface position between the solid and liquid phases is presented. Stability diagrams (V_{max}-Ha) and (Nu_{avg}-Ha) in each direction of magnetic field are obtained and discussed. We show that the strangest stabilization of the flow field and heat transfer is obtained when the magnetic field is applied in the horizontal direction Bx, and when all walls of the cubical enclosure are electrically conducting.

Keywords: Magnetic field, stability, natural convection, phase change.

1 Introduction

Phase change has a great importance in many industrial applications, e.g. in casting, solar energy, food processing, growth of single crystals from melts...etc. During the crystal growth by the horizontal Bridgman technique, sufficiently high variations in temperature can occur between the melt and the solidification front, which generate convective flows. Because of the appearance of striations which can affect the growth rate and structure of the solid and thus its quality, the convection and oscillatory instabilities can be eliminated by the application of a magnetic field (Hurle,1966).

[1] LEAP Laboratory, Dept. Mechanical Eng. University of Mentouri-Constantine, Algeria
[2] Dept. Mechanical , University of Laghouat, Algeria

Many researchers have done a large number of studies of natural convection in cavities (Achoubir et al.,2008; Bucchignani et al., 2009;Djebali et al., 2009; Mezrhab and Naji, 2009). Ben Hadid and Henry (1997) carried out a numerical study of the natural convection in a parallelepiped cavity for a highly conducting fluid with a given temperature distribution in presence of an external magnetic field. They show that the direction and the intensity of the magnetic field have an important influence on the flow evolution. Mössner and Müller (1999) highlighted the effect of Lorentz force on the organization of the flow and heat transfer, and observed a relative intensification of the flow in the corners of the cavity. They show that for orthogonal magnetic field to the isothermal walls is more efficient in influencing heat transfer and fluid flow. Juel et al. (1999) observed similar changes of structures from numerical and experimental results, traduced by a bidimensionnalization of the flow convection and a suppression of their oscillations, in a horizontally lengthened cavity filled by a gallium and exposed to uniform orthogonal magnetic field to the principal flow.

In a geometry similar to the horizontal Bridgman configuration for crystal growth, Bessaïh et al. (1999) studied numerically a combined effect of wall electrical conductivity and magnetic field orientation on the liquid metal flow. Fischer et al. (1999) investigated numerically and experimentally the effect of a rotating magnetic field on buoyancy-driven convection in Rayleigh-Bénard configuration, and the one Marangoni-convection in a floating zone configuration. The main important result of this study is that the temperature fluctuations caused by time-dependent buoyancy and Marangoni-convection can be damped by using a rotating magnetic field with relatively small field strength. Gelfgat and Yoseph (2001) studied numerically the effect of an external magnetic field on oscillatory instability of convective flow with different magnitudes and orientations in a rectangular cavity. Stability diagrams for the dependence of the critical Grashof number on the Hartmann number were obtained by the authors. They show that a vertical magnetic field provides a strongest stabilization effect, and also that the multiplicity of steady states is suppressed by the electromagnetic effect. Wang and Nobuko (2002) showed the strong dependence of magnetic damping of natural convection in low-conducting aqueous solution on the aspect ratio of a rectangular cavity. Burr et al. (2003) confirmed experimentally that for a large Hartmann number, there is a strong suppression of the convective flow, and the heat transfer is reduced to a purely conductive mode in a eutectic mixture of sodium potassium filled in a vertical cavity.

In the presence of magnetic field, Wen and Su (2005) studied experimentally the natural convection in a square Hele-Shaw cell with heat transfer measurements and liquid crystal thermography. They show that the vertically imposed magnetic field has a destabilizing influence, and that the flow instability modes become different

from that in two-dimensional cavity cases with and without magnetic field, where a pair of symmetric counter-rotating vortices is observed for the 2D instability mode. Hennenberg et al. (2005) showed that an analysis of the Rayleigh–Bénard–Marangoni problem of a ferrofluid submitted to a weak magnetic field needs a very argumented choice for proper scaling, when the width of the layer is larger than the capillary length, so that the Kelvin term intervenes in the momentum balance. Xu and Stock (2006) show experimentally that the natural convection in a Gallium contained in a rectangular box with the two opposite vertical walls held at different temperatures is suppressed with an imposed magnetic field, and the damping effect increases with a strength magnetic field.

The study of convective flow suppression has not been limited to magnetic suppression only; electric and electromagnetic field have also been applied to control the flow field. Kaneda et al. (2006) related the effect of an electrical current on the natural convection of a liquid metal under a uniform magnetic field in a cubic cavity. Their results show that, when only a magnetic field applied parallel to the heated and cooled walls, the natural convection is deadened by the Lorentz force. However, when electrical current and a magnetic field are applied, the heat transfer rate of the heated wall toward the cooled wall differs with the case in which only a magnetic field is applied. Kader et al. (2007) focused their attention on two major effects influenced by forced convection induced by a traveling magnetic field: the macro-segregation and the grain structure for Al-Ni alloys. They show that this configuration can control macro-segregations and that, moreover, the dendritic primary spacing may be modified by varying the applied field. They show that the effect of the traveling magnetic field on the constitutional under-cooling and on the refiner distribution induces a directional to an elongated transition. Recently, Kolsi et al. (2007) carried out a numerical study of natural convection in a differentially heated cubic cavity for Pr=0.045 under the presence of an external magnetic field orthogonal to the isothermal walls. They observed a damping and laminarization effects of the external magnetic field, and an organization of the central three-dimensional motion. Battira and Bessaïh (2009) show that the effect of a magnetic field in either the longitudinal or vertical direction provides a notable change on the flow and thermal structures of three-dimensional natural convection in the horizontal Bridgman configuration. Also, wall electrical conductivity has an effect on the average Nusselt number. Schwesig et al. (2004) showed numerically that the use of traveling magnetic field offers in contrary to the one rotating a significant improvement with respect to the bending of the solid/liquid interface as well as the resulting thermo-elastic stress and stability of the flow regime in the vertical gradient freeze growth of InP crystals. Lantzsch et al. (2008) showed that in growth of Ge crystals in doped vertical gradient freezing (VGF) with traveling

magnetic field (TMF) has a considerable effect on the deflection of the solid–liquid interface, whereas the doping segregation does not change significantly compared to the growth without magnetic field.Very recently, Mechighel et al. (2009) carried out a numerical study to investigate the three-dimensional buoyant flow in a parallelepiped box heated from below and partially from the two sidewalls. The influence of an applied horizontal magnetic field on the stability properties of the flow has been considered. Numerical and experimental study of forced mixing with static magnetic field on SiGe system has been carried out by Armour and Dost (2009). The 3-D numerical simulation results verify the experimental observations and show that the flow structure of the melt has dramatically changed under the effect of magnetic field.

In the present work, the magnetohydrodynamics stability with phase change (solidification) in a cubical enclosure is studied. The cubical enclosure heated from one vertical wall and cooled from an opposing wall is used as a benchmark system. We applied an external magnetic field in horizontal, vertical, and transversal directions separately; and we consider two electric potential boundary conditions: electrically conducting and insulating walls. The shape and the interface location of phase change are intended with and without magnetic field, and stability diagrams are obtained. We note that the interface location of three-dimensional flows has almost never been considered, exception the recent study of Douglas et al. (2005). Section 2 presents the mathematical formulation. Section 3 discusses the numerical method and techniques, which have been used for the computation, the grid independence study, and the comparison between our predictions and the experimental results found in the literature. Section 4 presents the results and discussion. Finally, a conclusion is given.

2 Problem statement and mathematical formulation

The physical system for the problem under consideration, as shown in Figure 1, is a cubical enclosure of length L, which contains a liquid metal (Gallium) characterized by a low Prandtl number (Pr=0.020). The left and right vertical walls are maintained at a local hot temperature T_h ($T_h > T_m$) and a local cold temperature T_c ($T_c < T_m$), respectively, where T_m=302.78 K is the melting temperature. The other walls are adiabatic. A uniform magnetic field is applied in three-directions Bx, By, and Bz separately.The interaction between the magnetic field and the flow field involves an induced electric current density $\vec{j}$, defined as (Moreau,1990):

$$\vec{j} = \sigma \left[-\vec{\nabla}\varphi + \vec{V} \times \vec{B} \right] \tag{1}$$

Where $\vec{V}$ is the velocity vector and $\vec{B}$ is the magnetic flux density vector. The

divergence of Ohm's low, $\nabla.\vec{j} = 0$, produces the equation of the electric potential φ:

$$\nabla^2\varphi = \vec{\nabla}\left(\vec{V} \times \vec{e}_B\right) \tag{2}$$

$\vec{e}_B$ is the unitary vector of the direction of $\vec{B}$. By neglecting the induced magnetic field, the dissipation and Joule heating, and using L, ν_l/L, l^2/ν_l, $\rho\,(\nu_l/L)^2$, $\nu_l B_0$, $(h_h - h_C)$ as typical scales for lengths, velocities, time, pressure, potential, and enthalpy , respectively.

The thermo-physical and electrical proprieties of the Gallium used in this study are given in Ref. (Metal Handbook, 1990) and the work of Douglas et al. (2005).

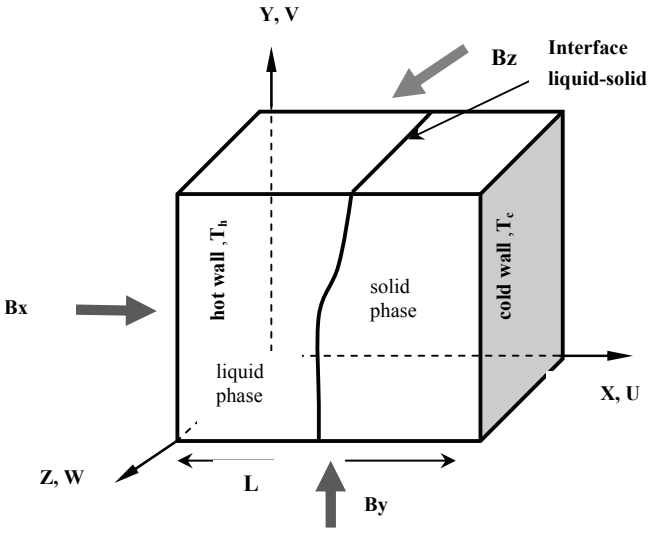

Figure 1: A cubical enclosure

2.1 Governing equations

For an incompressible flow considering a phase-change problem, Newtonian fluid with the Boussinesq approximation are described by the continuity and Navier-Stokes equations coupled with the energy equation, in the Cartesian coordinates system (X, Y, and Z), written in dimensionless as follows:

Continuity equation:

$$\frac{\partial U}{\partial X} + \frac{\partial V}{\partial Y} + \frac{\partial W}{\partial Z} = 0 \tag{3}$$

X-momentum equation:

$$\frac{\partial U}{\partial \tau}+\frac{\partial (UU)}{\partial X}+\frac{\partial (VU)}{\partial Y}+\frac{\partial (WU)}{\partial Z}=$$

$$-\frac{\partial P}{\partial X}+\frac{\partial^2 U}{\partial X^2}+\frac{\partial^2 U}{\partial Y^2}+\frac{\partial^2 U}{\partial Z^2}+F_{EMX}+S_U \tag{4}$$

Y-momentum equation:

$$\frac{\partial V}{\partial \tau}+\frac{\partial (UV)}{\partial X}+\frac{\partial (VV)}{\partial Y}+\frac{\partial (WV)}{\partial Z}=$$

$$-\frac{\partial P}{\partial Y}+\frac{\partial^2 V}{\partial X^2}+\frac{\partial^2 V}{\partial Y^2}+\frac{\partial^2 V}{\partial Z^2}+Gr.\theta+F_{EMY}+S_V \tag{5}$$

Z-momentum equation:

$$\frac{\partial W}{\partial \tau}+\frac{\partial (UW)}{\partial X}+\frac{\partial (VW)}{\partial Y}+\frac{\partial (WW)}{\partial Z}=$$

$$-\frac{\partial P}{\partial Z}+\frac{\partial^2 W}{\partial X^2}+\frac{\partial^2 W}{\partial Y^2}+\frac{\partial^2 W}{\partial Z^2}+F_{EMZ}+S_W \tag{6}$$

In eqs. (3), (4), (5), and (6), F_{EMX}, F_{EMY}, F_{EMZ} , U, V, and W are the dimensionless components of the Lorentz force and dimensionless components of the velocity in the X-,Y-,and Z- directions, respectively. Expressions of the Lorentz forces F_{EMX}, F_{EMY}, and F_{EMZ} for each direction of the magnetic field are obtained in detail in the work of Bessaïh et al. (1999). The Hartmann and Grashof numbers are defined, respectively, as:

$$Ha = B.L\sqrt{\sigma/\rho.\nu_l} \tag{7}$$

$$Gr = \frac{\rho_l g \beta_l (T_h - T_c) L^3}{\nu_l^2} \tag{8}$$

Where g is the magnitude of gravitational acceleration, β_l the thermal expansion coefficient of the fluid,ν_l the kinematical viscosity of the fluid, ρ_l the density, and σ the electrical conductivity of the fluid. The Darcy termsS_U, S_V and S_W are defined, respectively, as (Sin et al. 2001):

$$S_U = -\xi \frac{(1-f_l)^2}{\left(f_l^3+\varepsilon\right)} U \tag{9a}$$

$$S_V = -\xi \frac{(1-f_l)^2}{\left(f_l^3+\varepsilon\right)} V \tag{9b}$$

$$S_W = -\xi \frac{(1-f_l)^2}{(f_l^3+\varepsilon)} W \tag{9c}$$

These terms are necessary for the suppression of velocities U, V and W, when the control volume is occupied by the solid phase. The values of $\xi = 10^9 \mathrm{Kg/m^3}$ and $\varepsilon = 0.005$ are constants, which were used in the work of Sin et al. (2001). The enthalpy method is introduced and the expressions of the liquid fraction f_l in the solid, liquid and mushy regions are given in detail in our previous study (Bessaïh and Bouabdallah, 2008):

$$f_l = \begin{cases} 0 & h_S \le C_S T_m \\ (h - C_S T_m)/L_V & C_S T_m < h < C_S T_m + L_V \\ 1 & h \ge C_S T_m + L_V \end{cases} \tag{10}$$

Energy equation (enthalpy):

$$\frac{\partial \hbar}{\partial \tau} + \frac{\partial (U\hbar)}{\partial X} + \frac{\partial (V\hbar)}{\partial Y} + \frac{\partial (W\hbar)}{\partial Z} =$$
$$\frac{C}{Pr}\left\{\frac{\partial}{\partial X}\left[K\frac{\partial \hbar}{\partial X}\right] + \frac{\partial}{\partial Y}\left[K\frac{\partial \hbar}{\partial Y}\right] + \frac{\partial}{\partial Z}\left[\frac{\partial \hbar}{\partial Z}\right]\right\} +$$
$$+\frac{C}{Pr}\left\{\frac{\partial}{\partial X}\left[K\frac{\partial (\hbar_S - \hbar)}{\partial X}\right] + \frac{\partial}{\partial Y}\left[K\frac{\partial (\hbar_S - \hbar)}{\partial Y}\right]\right\} +$$
$$+\frac{C}{Pr}\left\{\frac{\partial}{\partial Z}\left[\frac{\partial (\hbar_S - \hbar)}{\partial Z}\right]\right\} \tag{11}$$

Where $C = C_l/C_s$ represents the ratio of specific heats of the liquid phase to the solid phase, $Pr = \nu_l/\alpha_l$ is the Prandtl number, and K is the ratio of the thermal conductivity of the solid phase to the liquid phase:

$$K = \begin{cases} \frac{k_s}{k_l} = \frac{70.98[W.m^{-1}.K^{-1}]}{31.24[W.m^{-1}.K^{-1}]} = 2.271 & \text{In the solid phase} \\ \frac{k_l}{k_l} = \frac{31.24}{31.24} = 1 & \text{In the liquid phase} \end{cases}$$

2.2 Initial and Boundary conditions

The governing equations (3) –(6) and (11) are subject to the following dimensionless initial and boundary conditions: At: $\tau = 0$:

$$U = V = W = 0, \quad \theta = \hbar = 1 \tag{12a}$$

For $\tau > 0$:

$$X = 0: \quad U = V = W = 0, \quad \hbar = 1 \tag{12b}$$

$$X = A: \quad U = V = W = 0, \quad \hbar = 0 \tag{12c}$$

$$Y = 0: \quad U = V = W = 0, \quad \frac{\partial \hbar}{\partial Y} = 0 \tag{12d}$$

$$Y = 1: \quad U = V = W = 0, \quad \frac{\partial \hbar}{\partial Y} = 0 \tag{12e}$$

$$Z = 0: \quad U = V = W = 0, \quad \frac{\partial \hbar}{\partial Z} = 0 \tag{12f}$$

$$Z = 1: \quad U = V = W = 0, \quad \frac{\partial \hbar}{\partial Z} = 0 \tag{12g}$$

In addition, for the electric potential boundary conditions on the walls of the enclosure are:

- Electrically conducting walls: $\varphi = 0$.
- Electrically insulating walls: $\partial\varphi/\partial n = 0$, where n is the normal on the wall considered.

3 Numerical method

The governing equations (3) – (6) and (11), with the associated boundary conditions (12a-g), were solved by using the finite-volume method, as described by Patankar (1980). The components of the velocity (U, V and W) are stored at staggered locations, and the scalars quantities (P, θ, φ and $\hbar$) are stored in the centers of these volumes. The numerical procedure called SIMPLER algorithm (Patankar,1980) is used to handle the pressure–velocity coupling. The second-order-accurate central difference scheme is used to discretize the convection and diffusion terms. This approach was utilized successfully by Zhou and Zebib (1992). The discretized algebraic equations are solved by the line-by-line tridiagonal matrix algorithm (TDMA). Convergence at a given time step is declared when the maximum relative change between two consecutives iterations levels fell below 10^{-4} for U,V,W and $\hbar$. At this stage, the steady-state solution is obtained. A parallel test was made to guarantee that the energy balance between the hot and cold walls is less than a prescribed accuracy value, i.e., 0.2%. Calculations were carried out on a PC with a 3GHz CPU, and the average computing time for a typical case was approximately 24hours. The numerical solution is obtained as follows:

Step. 1: Give the initial values of U, V, W and $\hbar$.

Step. 2: Predict F_{EMX}, F_{EMY}, F_{EMZ}, S_U, S_V and S_W, according to Esq. (9a), (9b), and (9c).

Step. 3: Solve Eqs. (3)–(6) and (11) for U, V, W and $\hbar$.

Step. 4: If the convergence is achieved, repeat steps 2 and 3 for the next time step.

3.1 Grid Independence Study

Three uniform grids were used in order to determine the appropriate grid size: 36×36×36, 52×52 ×52, and 82× 82×82 nodes. In Figures 2a-c, we have presented the evolution of the vertical and horizontal velocity and the temperature in X-direction at the middle of the enclosure at Y=0.5 and Z=0.5. The dimensionless temperature θ is scaled by the temperature difference between the hot and cold walls ($T_h - T_c$). These Figures show a small difference between the grids sizes. The influence of grid size on the interface location X_{int} is shown in Table 1. In order to optimize the CPU time and the cost of computations, the grid corresponding to 52×52 ×52 nodes is used for all simulations, as a result of performing grid independence tests.

Table 1: Interface location (X_{int}), for three grids size.

Interface location, X_{int}	Grid 36×36×36	Grid 52×52 ×52	Grid 82× 82×82
(Y=0,Z=0.5)	0.58483	0.59841	0.59790
(Y=0.5,Z=0.5)	0.63500	0.62912	0.64030
(Y=1,Z=0.5)	0.68016	0.66013	0.67749
(Y=0.5,Z=0)	0.61931	0.62251	0.63499
(Y=0.5,Z=1)	0.61931	0.62251	0.63499

3.2 Validation of the computer code

A first comparison between our predictions and the experimental data of Beckerman and Viskanta (1989) is presented in Figure 3, which shows a dimensionless temperature distribution in the enclosure at Y= 0.133, 0.5, and 0.867. A good agreement is observed with the work of Beckerman and Viskanta (1989). A second comparison is presented in Table 2 between our numerical results and the predictions of Douglas et al. (2005) of the interface location (X_{int}) for Pr=0.020 and Gr=8.0358×10^4. A good agreement is obtained with the work of Douglas et al. (2005).

4 Results and discussion

We fixed the Grashof number at Gr=10^5, Prandtl number at Pr=0.020, and we varied the Hartmann number from 0 to 200. In the absence of magnetic field the Hartmann number, Ha=0. However, in the presence of magnetic field, Ha≠0, which is

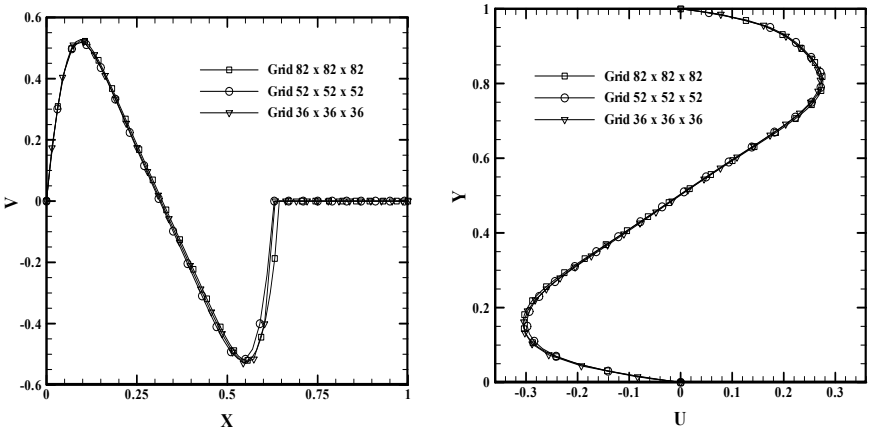

(a) Vertical velocity V **(b)** Horizontal velocity U

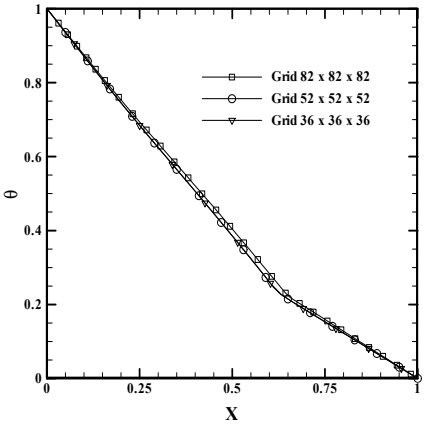

(c) Temperature Θ

Figure 2: Evolution of the vertical velocity V, horizontal velocity U, and the temperature θ at middle of the enclosure for different grids size and Gr=10^5

oriented in X-direction Bx, in Y-direction By, and in Z-direction Bz separately. A dimensionless time step is equal to $\Delta\tau$=10^{-5} , which is used in all simulations, and the variables U, V, W, $\hbar$ and φ are presented in dimensionless form.

4.1 Flow field

The situation considered herein is a very important example of convective circulation inside an enclosed region, in which vertical hot and cold walls contribute in driving the flow in the melting region.

Table 2: Comparison of the interface location X_{int} between our study and the predictions of Douglas et al. (2005).

Interface location, X_{int}	Douglass et al. (2005)	Present work
(Y=0, Z=0.5)	0.60706	0.59798
(Y=0.5,Z=0.5)	0.62684	0.62716
(Y=1, Z=0.5)	0.66000	0.66149
(Y=0.5, Z=0)	0.62684	0.61916
(Y=0.5,Z=1)	0.62684	0.61916

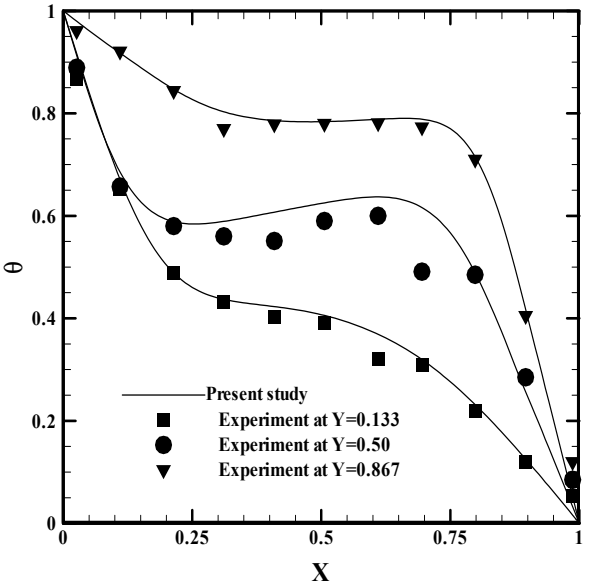

Figure 3: Temperature distribution θ: Comparison between our numerical results and the experimental data of Beckerman and Viskanta (1989)

In the absence of magnetic field, Ha=0, Figure 4a shows the horizontal distribution of the components of the velocity (U, V, and W) in the middle of the enclosure at Y=0.5 and Z=0.5 for Gr=10^5. We can see the change the magnitude of velocities in the liquid part of the enclosure, and a strong change in value appearing in the vertical velocity V. The horizontal velocity U changes from -0.15 to 0.05 and the V changes from -0.55 to 0.55, but no-change in the transversal velocity W. The similar change is observed for the temperature in X-, Y-, and Z-directions (Fig.4b). The strongest change in the temperature appears in X-direction. We can

concluded that the two-dimensional solution provides only an approximation of the problem physics. All the movement of phase change are due to the gravitational force (natural convection) created in the fluid part of the enclosure. These results are confirmed in the work of Semma and El-Ganaoui (2003) and Douglass et al. (2005).

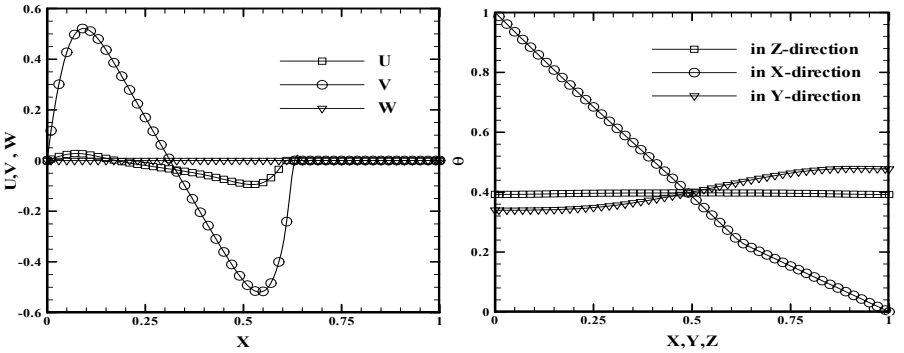

(a) Components of the velocity U, V, W **(b)** Temperature Θ

Figure 4: Evolution of the velocity components (U, V, W) and temperature in the middle of the enclosure for Gr=10^5 and Ha=0

Figures 5a-d show the velocity-vectors in the enclosure for Gr=10^5 and various values of the Hartmann number. For Ha= 0 (Fig. 5a), it is clear from this figure, which show a single clockwise-rotation convection cell, that the fluid in the liquid phase rises along the hot wall (at X=0) and then circulates towards the solid phase along which it falls and circulates towards hot wall. In the center of this convection cell, the velocities have a lower magnitude. In the solid region, there is no movement of the fluid. The velocities of the fluid in the boundary layers near the hot wall and solid phase are higher than the velocities along the horizontal top and bottom walls; a similar variation was founded by Wolff et al. (1988) in their numerical simulation of natural convection of liquid metals in vertical cavities.

When the magnetic field is applied in three-directions separately and for Ha=50 (Figs. 5b-d), the magnitude of velocity-vectors decreases from Bz to Bx. So that, the strongest stabilization effect in the velocity field is achieved when the magnetic field is applied in the X-direction. This has been experimentally and numerically verified by many studies (Dost et al. 2002; Liu et al. 2002; Sheibani et al. 2003; Dost et al., 2003; Liu et al. , 2004).

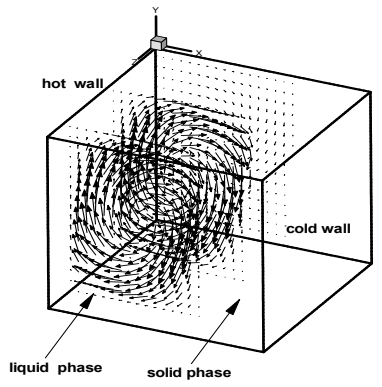

(a) Ha=0 (without magnetic field)

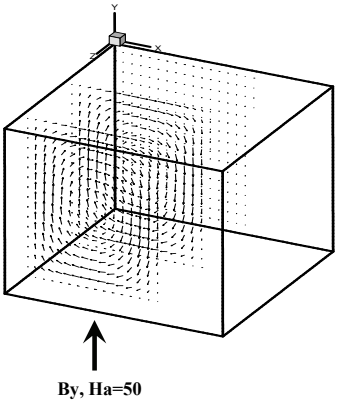

(c) Y-magnetic field, By

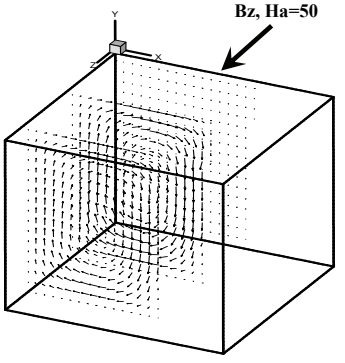

(b) Z-magnetic field, Bz

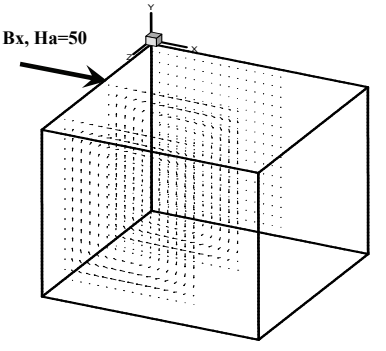

(d) X-magnetic field, Bx

Figure 5: Velocity-vectors in the enclosure for three-directions of magnetic field, and for Gr=10^5 and Ha= 50

4.2 Phase field

The characteristics of this problem are such that the interface location is a good measure of phase change, because at a strong magnetic field, the processes essentially become conductive (Grandet and Alboussiere,1999). The interface location in 3D flow is fully implicit, as presented in Figure 6a, for Gr=10^5 and various values of the Hartmann number (Figs.6b-c) . For Ha=0 (Fig. 6a), the shape of the interface becomes inclined surface in the better side of the enclosure. The interface

is placed between X= 0.59 and 0.66, Y= 0 and 1, Z=0 and 1. This shape is caused by the convection flow in the liquid part of the enclosure, and is better developed in the bottom wall by buoyancy force. When the magnetic field is applied in the horizontal direction Bx and for Ha=25, the interface location is developed by change in their location, stabilized between X= 0.60 and 0.64, Y= 0 and 1, Z=0 and 1 (Fig. 6b) , for Ha= 50 between X= 0.61 and 0.63, Y= 0 and 1, Z=0 and 1 (Fig. 6c) , and finally for Ha= 100 at X= 0.62, Y= 0 and 1 , Z=0 and 1 (Fig. 6d). We conclude that the horizontal magnetic field Bx removes the natural convection flow and stabilizes the shape of the interface for high values of the Hartmann number, and the shape of the interface between the liquid and solid phases is depended to the magnitude and orientation of magnetic field.

4.3 Thermal field

Figures 7a-d show four iso-surfaces of the temperature (θ= 0.8, θ = 0.6, θ = 0.4 and θ = 0.25) at different locations of the enclosure, for Gr=10^5 and various values of the Hartmann number (Ha=0, 25, 50, and 100). The dimensionless melting temperature of the molten Gallium, $\theta = \theta_m$ =0.25. For Ha= 0 (Fig. 7a), we can see a distortion of the temperature, decreasing in the left iso-surface (liquid part) to the one right (solid part).This effect is produced efficiently by the natural convection in molten Gallium and the pure heat conduction in the solid phase. The heat is transferred from the hot wall to the cold wall by convection and diffusion in the liquid phase.

When the magnetic field is applied in the X-direction and the Hartmann number increases from 25 to Ha=100 (see Figs. 7b-d), we can see a disappearance of the stratification and stabilization of temperature fields, which become parallel to the vertical walls, indicating the dominance of conduction mode. It is noticed that, the magnetic field Bx in X-direction and when all walls are electrically conducting, corresponding the major conditions of stabilization (see, the stability diagrams in section 4.6). This result is similar to the one of Kolsi et al. (2007), and Battira and Bessaih (2008). Then, the effect of magnetic field stabilizes the thermal fields by the suppression of convection in melt part of the enclosure.

4.4 local Nusselt number

The iso-contours of the local Nusselt number on the hot wall in the Y-Z plane of the enclosure is represented in Figure 8, for Ha=50 and three-directions of magnetic field. Here, all walls are electrically conducting. It is shown that, the variations according to Y-direction are attenuated in the presence of magnetic field. This involves an important two-dimensionalization of heat transfer. At Ha=0 (Fig.8a), the maximum value of the local Nusselt number Nu (defined as: $Nu = -\partial\theta/\partial X$) is

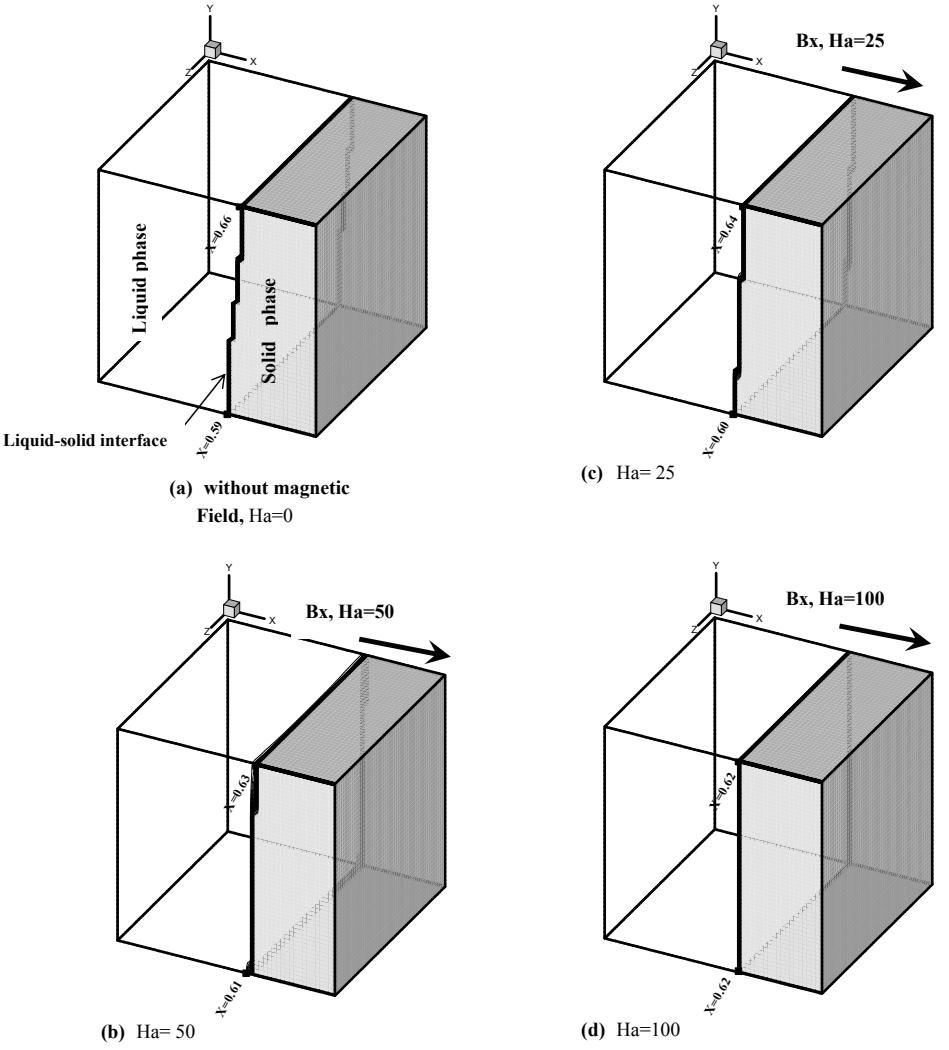

Figure 6: The phase field without and with magnetic field for Ha=0, 25, 50 , and 100, and Gr=10^5 . Here, the magnetic is applied only in X-direction Bx , and all walls are electrically conducting walls

1.6, which decreases to 1.30 for Ha=50 when the magnetic field is oriented in the horizontal direction (Fig.8b), and 1.375 when the vertical magnetic field is oriented vertically (Fig.8c), and finally to 1.40 when the magnetic is applied in transversal direction (Fig.8d). This analysis signifies that the horizontal magnetic field Bx reduces the heat transfer more than the vertical magnetic field By and transver-

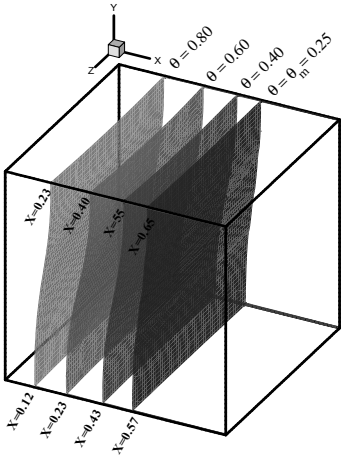

(a) Without magnetic field, Ha=0

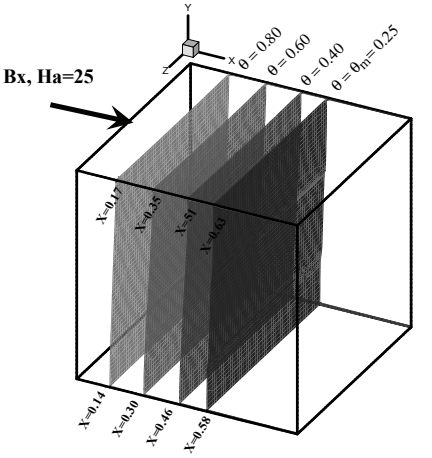

(b) Ha=25

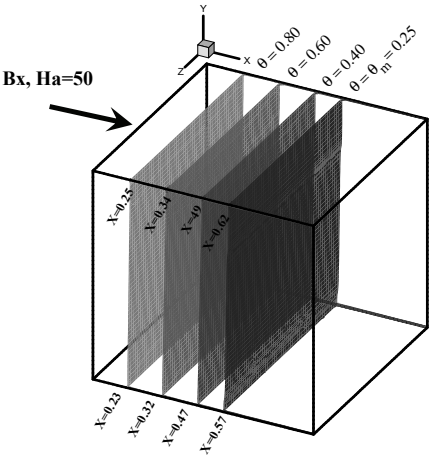

(c) Ha=50

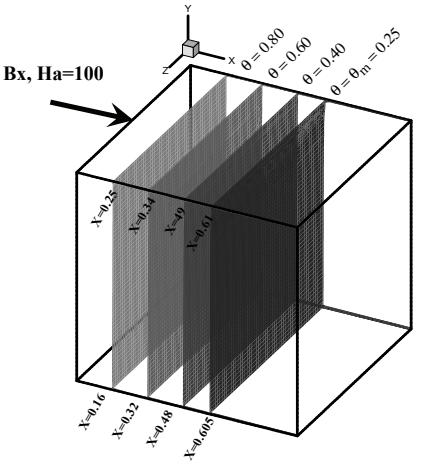

(d) Ha=100

Figure 7: Iso-surfaces of temperatures for Gr=10^5 and various Hartmann numbers, Ha=0, 25, 50 , and 100. The magnetic field Bx is applied in X-direction, and all walls are electrically conducting.

sal magnetic field Bz. In conclusion, the important reduction of heat transfer is obtained with the application of a horizontal magnetic field Bx.

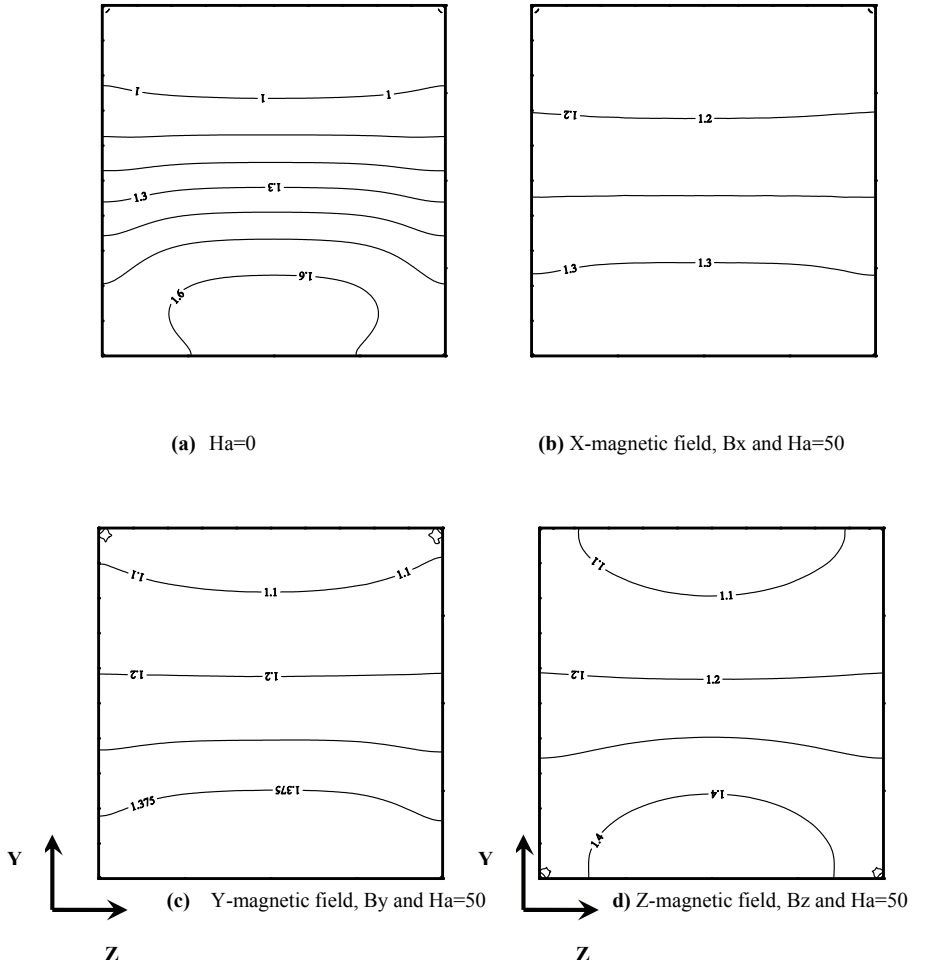

(a) Ha=0

(b) X-magnetic field, Bx and Ha=50

(c) Y-magnetic field, By and Ha=50

d) Z-magnetic field, Bz and Ha=50

Figure 8: Iso-contours of local Nusselt numbers on the hot wall for Gr=10^5, various values of the Hartmann number Ha=0 and 50, and three-directions of magnetic field Bx, By, and Bz.

4.5 Potential field

To illustrate the three-dimensional electro-magnetically character of this problem, we have plotted in Figures 9a-c the iso-surfaces of electric potential in the (X-Y)

plane at the middle of the enclosure. The magnetic field is applied in X-, Y-, and Z directions separately, the Hartmann number is fixed to Ha=50 and the case of electrically insulating walls is considered. We can see a different distribution of iso-surfaces and a dependence of the structure of iso-lines with change of direction of magnetic field.

The interaction between the convective flows and electromagnetically field can be explaining by the equation of potential Equation 2, re-written in explicit form below as:

$$\frac{\partial}{\partial X}\left(\frac{\partial \varphi}{\partial X}\right)+\frac{\partial}{\partial Y}\left(\frac{\partial \varphi}{\partial Y}\right)+\frac{\partial}{\partial Z}\left(\frac{\partial \varphi}{\partial Z}\right)=S_{\varphi}$$
$$S_{\varphi}=\begin{cases}\frac{\partial V}{\partial Z}-\frac{\partial W}{\partial Y}\\ \frac{\partial W}{\partial X}-\frac{\partial U}{\partial Z}\\ \frac{\partial U}{\partial Y}-\frac{\partial V}{\partial X}\end{cases} \tag{13}$$

In this equation, the right hand side contains the velocity gradients, In the solid phase, these velocity gradients are equal to zero, since the solid material held fixed. However, in the liquid phase these velocity gradients are present and contribute to the gradient of the electric potential distribution. A very good similarity can be observed with these results and of Gonçalves et al. (2005).

4.6 Stability diagrams

In Figures 10a-b, we have presented the stability diagrams (V_{max}-Ha) and (Nu_{avg}-Ha) when the magnetic field is applied in three-directions Bx, By, and Bz separately. Two cases of electric potential boundary conditions (electrically insulating and conducting walls) are considered. These diagrams show the dependence of the maximal velocity and average Nusselt number with the Hartmann number, the velocity is decreased when the Hartmann number is increased. The strongest damping of the flow and heat transfer is obtained when the magnetic field is applied in the X-direction, 5% high to the Y-direction and 9% high to the Z-direction, in the range of the Hartmann number (Ha < 200).

Figures 11a-b show a comparison between the stabilization effects in heat transfer (Nusselt number) by application of magnetic field in, Y-, and Z-directions separately. It is shown a low difference between the insulating and conducting walls. This difference increases when the magnetic field is applied in Y-direction, and slightly in Z-direction. The contribution of electric potential is significant. This has been supported by Yildiz et al. (2006).

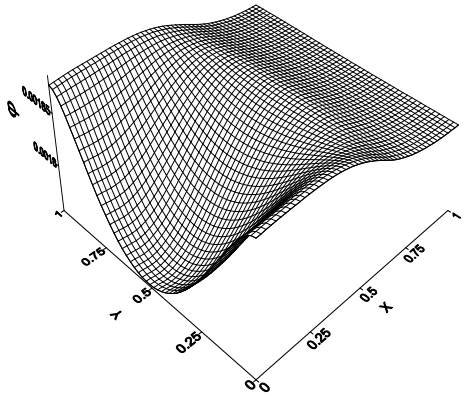

(a)X-magnetic field, Bx

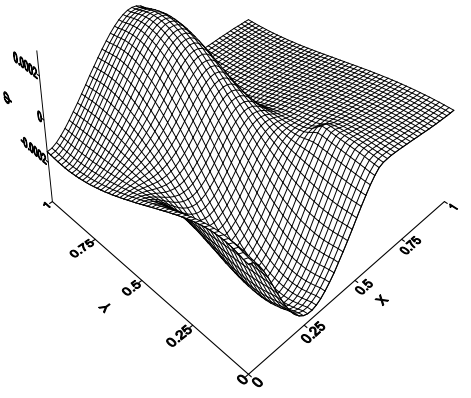

(b)Y-magnetic field, By

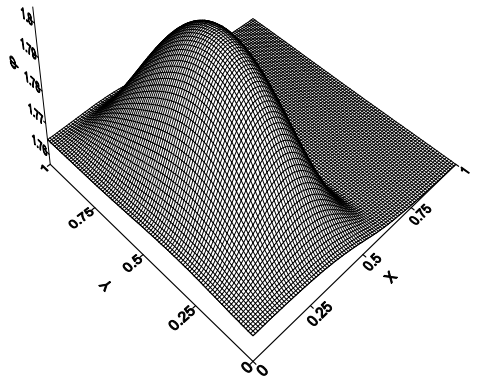

(c) Z-magnetic field, Bz

Figure 9: Electric potential field in the (X-Y) plane for Gr=10^5 and Ha=50. The magnetic field is applied in three-directions Bx, By, and Bz

5 Conclusion

Three-dimensional natural convection during the process of phase change (solidification) of a pure liquid metal in the cubical enclosure has been numerically studied with and without magnetic field, oriented in X-, Y-, and Z-directions separately. The finite-volume method has been used to solve the modeling equation, along with an enthalpy method, which has been used to determine the position of the interface between the solid and liquid phases. The Grashof number was fixed to 10^5 and the Hartmann number was varied from to 0 and 200. The main results obtained in this study are:

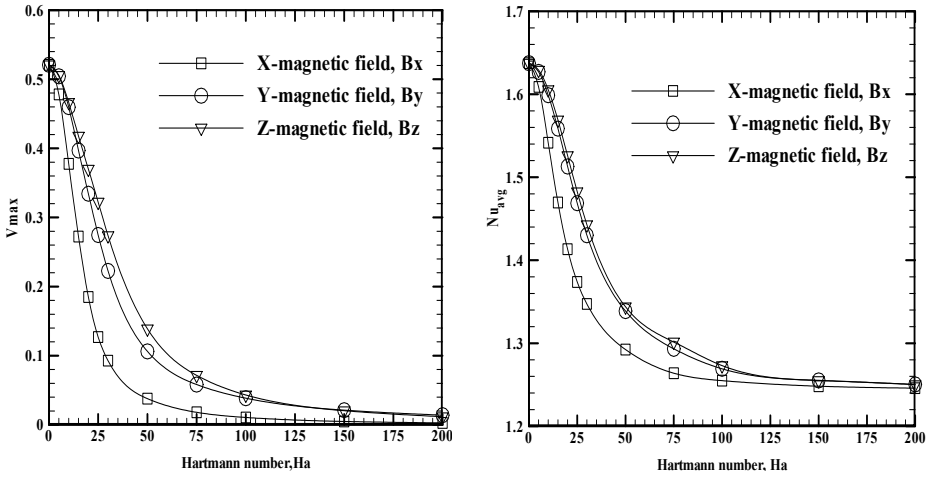

(a) (Vmax-Ha) **(b)** (Nu_{avg}-Ha)

Figure 10: Stability diagrams when all walls are electrically conducting. The magnetic field is applied in the three-directions Bx, By, and Bz separately.

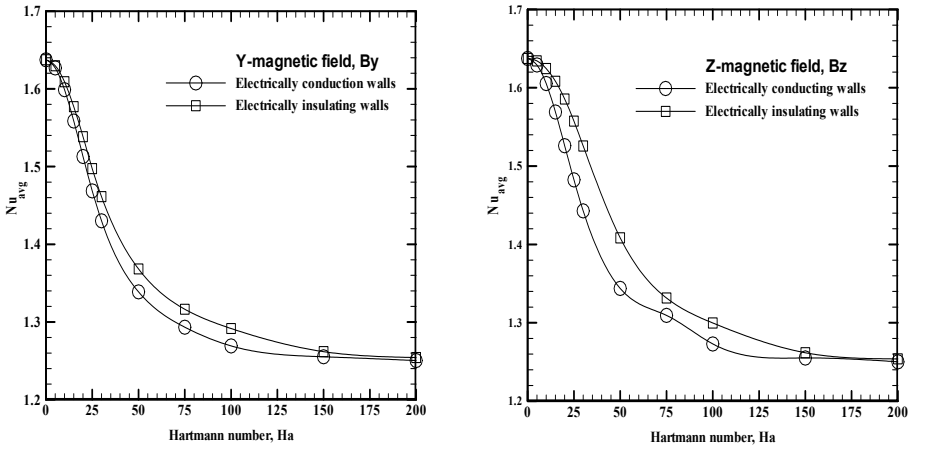

(a) Y-magnetic field, By (b) Z-magnetic field, Bz

Figure 11: Stability diagrams (Nu_{avg}-Ha) for the cases when all walls are electrically conducting and insulating.

- The applied magnetic field involves important regulation on the shape and the location of the interface between the liquid and solid phases.
- With high value of the Hartmann number, the convection in the liquid part is suppressed successively and the interface becomes regular.
- The magnetic field involves important two dimensionalization of heat transfer through the isothermal walls.
- Stability diagrams (V_{max}-Ha) and (Nu_{avg}-Ha) for each direction and electric potential conditions are determined. They show the strangest stabilization of the flow field and heat transfer, when the magnetic field is applied in the X-direction and when all walls are electrically conducting.

These results help the industrialists to known the shape of interface during the phase change of a liquid metal. A high quality of material is obtained by an external magnetic field, with predetermined intensity and orientation.

Nomenclature

B	magnetic field Tesla
C	specific heat J/Kg.K
E	dimensionless electrical field
F	dimensionless Lorentz force
f	dimensionless liquid fraction
Gr	Grashof number
g	acceleration of gravity m/s^2
Ha	Hartmann number
h	enthalpy J/kg
$\hbar$	dimensionless enthalpy
J	dimensionless density current
K	ratio of the thermal conductivity of the solid phase to the liquid phase
k	thermal conductivity W/m.K
L	length of the enclosure m
Nu	local Nusselt number
P	dimensionless pressure
Pr	Prandtl number
S	dimensionless source term
T	temperature K
U,V,W	dimensionless horizontal, vertical, transverse velocity, respectively.
X,Y, Z	dimensionless Cartesians coordinates

Greek Symbols

α	thermal diffusivity m^2/s
β	thermal expansion coefficient K^{-1}
ν	kinematic viscosity m^2/s
θ	dimensionless temperature
ρ	density of the fluid kg/m^3
σ	electrical conductivity $\Omega^{-1}.m^{-1}$
φ	dimensionless electric potential
τ	dimensionless time

Subscripts and Superscripts

avg	average value
h	hot wall
c	cold wall
l	liquid phase
s	solid phase
m	melting
max	maximal value
n	normal direction

References

Achoubir, K.; Bennacer, R.; Cheddadi, A.; El Ganaoui, M.; Semma, E. (2008): Numerical study of thermosolutal convection in enclosures used for directional solidification (Bridgman Cavity). *FDMP: Fluid Dynamics and Materials Processing*, Vol. 4, No. 3, pp. 199-210.

Armour, N.; Dost, S. (2009): Numerical and experimental study of forced mixing with static magnetic field on SiGe system. *FDMP: Fluid Dynamics and Materials Processing,* Vol. 5, No. 4, pp. 331-344.

Battira, M.; Bessaïh, R. (2009): Three-dimensional natural convection in the horizontal Bridgman configuration under various wall electrical conductivity and magnetic field. *Numerical Heat Transfer*, *Part A*, Vol. 55, pp. 58-76.

Beckerman, C.; Viskanta, R. (1989): Effect of solid subcooling on natural convection melting of a pure metal. *ASME Journal of Heat Transfer*, Vol. 111, pp. 416-423.

Ben Hadid, H.; Henry, D. (1997): Numerical study of convection in the horizontal Bridgman configuration under the action of a constant magnetic field, Part 2, three dimensional flows. *Journal of Fluid Mechanics,* Vol. 333, pp. 57–83.

Bessaïh, R.; Kadja, M.; Marty, Ph. (1999): Effect of wall electrical conductivity and magnetic field Orientation on liquid metal flow in geometry similar to the horizontal Bridgman configuration for crystal growth. *International Journal of Heat Mass Transfer,* Vol. 42, pp. 4345.

Bessaïh, R.; Bouabdallah, S. (2008): Numerical study of oscillatory natural convection during solidification of a liquid metal in a rectangular enclosure with and without magnetic field. *Numerical Heat Transfer*, *Part A,* Vol. 54, pp. 331-348.

Bucchignani, E. (2009): An implicit unsteady finite Volume formulation for natural convection in a square cavity. *FDMP: Fluid Dynamics and Materials Processing*, Vol. 5, No. 1, pp. 37-60.

Burr, U.; Barleon, L.; Jochmann, P.; Tsinober, A. (2003): Magnetohydrodynamics convection in vertical slot with horizontal magnetic field. *Journal of Fluid Mechanics*, Vol. 475, pp. 21–40.

Djebali, R.; El Ganaoui, M.; Sammouda, H.; Bennacer, R. (2009): Some benchmarks of a side wall heated cavity using Lattice Boltzmann approach. *FDMP: Fluid Dynamics and Materials Processing,* Vol. 5, No. 3, pp. 261-282.

Dost, S.; Liu, Y.C.; Lent, B. (2002): A numerical simulation study for the effect of applied magnetic field in liquid phase electroepitaxy. *Journal of Crystal Growth,* Vol. 240, No. 1-2, pp. 39-51.

Dost, S.; Liu, Y.C.; Lent, B.; Redden, R.F. (2003): A numerical simulation study for the effect of applied magnetic field in growth of CdTe crystals by the travelling heater method. *International Journal of Applied Electromagnetics and Mechanics*, Vol. 17, No. 4, pp. 271-288.

Douglas, V.L.; Gonçalves, E.; Faghri, M.; Asako, Y.; Charamchi, M. (2005): Phase change in three-dimensional rectangular cavity under electro-magnetically simulated low-gravity: side wall heating. *International Journal of Numerical Methods for Heat and Fluid Flow*, Vol. 15, pp. 710-739.

Fischer, B.; Friedrich, J.; Weidman; Müller, G. (1999): The uses of time-dependent magnetic fields for control of convective flows in melt growth configurations. *Journal of Crystal Growth* , Vol.198/199, pp. 170-175.

Gelfgat, A. Yu.; Bar-Yoseph, P. Z. (2001): The effect of an external magnetic field on oscillatory instability of convective flows in a rectangular cavity. *Physics of Fluids*, Vol. 13, pp. 2269–2279.

Grandet, J.P.; Alboussiere, T. (1999): Bridgman growth: Modeling and experi-

ments. *Progress in Crystal Growth and Characterization of Materials*, pp. 73-132.

Hennenberg, M.; Weyssow, B.; Slavtchev,S.; Alexandrov,V.; Desaived, Th. (2005): Rayleigh Marangoni–Bénard instability of a ferrofluid layer in a vertical magnetic field. *Journal of Magnetism and Magnetic Materials,* Vol. 289, 268–271.

Hurle, D. (1966): Temperature oscillations in molten metals and their relationship to growth striae in melt-grown crystals. *Phil. Mag.,* Vol. 13, pp. 305–310.

Juel, A.; Mullin, T.; Ben Hadid, H.; Henry, D. (1999): Magnetohydrodynaimcs convection in molten Gallium. *Journal of Fluid Mechanics*, Vol. 378, pp. 97–118.

Kaneda, M.; Tagawa, T.; Ozoe, H. (2006): Natural convection of liquid metal under a uniform magnetic with an electric current supplied from outside. *Experimental Thermal and Fluid Sciences,*Vol.30, pp. 243–252.

Kader, Z.; Nathalie M.N.; Moreau. R. (2007): Control of melt convection by a traveling magnetic field during the directional solidification of Al–Ni alloys. *Compte Rendu de Mécanique,* Vol. 335, pp. 330–335.

Kolsi, L.; Abidi, A.; Borjini, M.N.; Daous, N.; Ben Aissa, H. (2007): Effect of an external magnetic field on the 3-D unsteady natural convection in a cubical enclosure. *Numerical Heat Transfer A*, Vol. 51, pp. 1003–1021.

Lantzsch, R.; Grants, I.; Patzold, O.; M. Stelter, M.; Gerbeth, G. (2008): Vertical gradient freeze growth with external magnetic fields. *Journal of Crystal Growth,* Vol. 310, pp. 1518–1522.

Liu, Y.C.; Okana, Y.; Dost, S. (2002): The effect of applied magnetic field on flow structures in liquid phase electroepitaxy-A three-dimensional model. *Journal of Crystal Growth*, Vol. 244, pp. 12-26.

Liu, Y.C.; Dost, S.; Sheibani, H. (2004): A three-dimensional simulation for the transport structures in liquid phase electroepitaxy under applied magnetic field. *International Journal of Transport Phenomena*, Vol. 6, pp. 51-62.

Mechighel, F.; El. Ganaoui, M.; Kadja, M.; Pateyron, B.; Dost, S. (2009): Numerical simulation of three-dimensional low Prandtl liquid flow in a parallelepiped cavity under an external magnetic field. *FDMP: Fluid Dynamics and Materials Processing,* Vol. 5, No. 4, pp. 313-330.

Metals Handbook. (1990): *Properties and Selection: Nonferrous Alloys and Special- Purpose Materials*, 10th ed. Vol. 2, ASM International, Chicago, IL, pp.1114-5.

Mezrhab, A.; Naji, H. (2009): Coupling of Lattice Boltzmann equation and finite Volume method to simulate heat transfer in a square cavity. *FDMP: Fluid Dynamics and Materials Processing*, Vol. 5 No. 3, pp. 283-296.

Moreau, R. (1990): *Magnetohydrodynamics.* Kluwer Academic Publisher.

Mössner, R.; Müller, U. (1999): A numerical investigation of three-dimensional magneto-convection in rectangular cavities. *Int. J. Heat Mass Transfer*, Vol. 42, pp. 1111–1121.

Patankar, S.V. (1980): *Numerical Heat Transfer and Fluid Flow*. McGraw-Hill, New York.

Schwesig. P.; Hainke, M.; Friedrich, J., Mueller, G. (2004): Comparative numerical study of the effects of rotating and travelling magnetic fields on the interface shape and thermal stress in the VGF growth of InP crystals. *Journal of Crystal Growth,* Vol. 266, pp. 224–228.

Semma, E.; El Ganaoui, M.; Cheddadi, A.; Bontoux, P. (2003): Instability of melt flow and solidification front during horizontal growth. *Congrès de Mécanique*, Vol. 331, pp. 631-639.

Sheibani, H.; Liu, Y.C.; Sakai, S.; Lent, B.; Dost, S. (2003): The effect of applied magnetic field on the growth mechanisms of liquid phase electroepitaxy. *International Journal of Engineering Sciences*, Vol. 41, pp. 401-415.

Sin, K.; Anghaie, S.; Chen, G. (2001): A fixed-grid two-phase numerical model for convection-dominated melting and solidification. *Proceedings First MIT. Conference on Computational Fluid and Solid Mechanics*. MIT. Cambridge. MA.

Wang, L.B.; Nobuko, I.W. (2002): Dependence of aspect ratio on magnetic damping of natural convection in low-conducting aqueous solution in a rectangular cavity *International Journal of Heat and Fluid Flow*, Vol.23, pp. 92-95.

Wen, C.Y.; Su, W.P. (2005): Natural convection of magnetic fluid in a rectangular Hele-Shaw cell. *Journal of Magnetism and Magnetic Materials,* Vol. 289, 299–302.

Wolff, F.; Beckermann, C.; Viskanta, R. (1988): Natural convection of liquid metals in vertical cavities. *Experimental Thermal and Fluid Science*, Vol. 1, pp.83-91.

Xu, B.; Li, Q.; Stock, D. E. (2006): An experimental study of thermally induced convection of molten Gallium in magnetic fields. *International Journal of Heat and Mass Transfer*, Vol. 42, pp. 2009–2019.

Yildiz, E.; Dost, S.; Yildiz, M. (2006): A numerical simulation study for the effect of magnetic fields in liquid phase diffusion growth of SiGe single crystals. *Journal of Crystal Growth*, Vol. 291, pp. 497-511.

Zhou, H.; Zebib, A. (1992): Oscillatory convection in solidifying pure metals. *Numerical Heat Transfer*, *Part A,* Vol. 22, pp. 435-468.